# µ-Photoluminescence imaging setup for optical characterisation of ZnO-based microcavities

M. Thunert, T. Michalsky, M. Wille, S. Richter, H. Franke, C. Sturm, R.Schmidt-Grund, M. Grundmann
Semiconductor Physics Group, Leipzig University, Leipzig, Germany (August 2014)

## Application Note

### Introduction

We present our experimental imaging setup for investigation of the photoluminescence (PL) emitted from ZnO-based semiconductor microcavities (MCs). Thereby, we use the Andor Solis Software in combination with the Ikon-M DU934P-BU2 camera to record two-dimensionally resolved images of the near-field as well as the far-field emission to achieve spatial or angular resolution of the PL distribution.

In general, a MC consists of a cavity layer which contains an active medium surrounded by highly reflective mirrors, often realized by distributed Bragg reflectors (DBR). This causes standing electromagnetic waves inside the cavity and hence a long lifetime of light in these structures. The electromagnetic field is one-dimensionally confined within the cavity layer for planar MCs, and two-dimensionally for geometries based on micro- and nanowires. The photonic eigenmmodes can be of Fabry-Pérot type (FPM) or, especially in wire structures, whispering gallery modes (WGM) which are confined by total internal reflections and a closed round trip of the wave within the wire cross section [1]. These modes can be occupied by so-called cavity-photons, which have, due to their tiny effective mass, a steep parabola-like dispersion:

$$E(k) = \frac{(hk)^2}{8\pi \mathrm{m}}$$

Here, E is the cavity-photon energy, h the Planck constant and m the effective photon mass. The in-plane wave-vector k = ($k_x$,$k_y$) is directly related to the emission angles ($\vartheta$, $\varphi$) via

$$k = (k_\mathrm{x}, k_\mathrm{y}) = \frac{2\pi\, E\,(\vartheta\varphi)}{hc}\ \sin(\vartheta\varphi)$$

where c is the velocity of light.

The photonic cavity modes can couple to the electronic system of the active medium (e.g. a semiconductor material) which is placed in the cavity. Two regimes of light-matter interaction can be realized, depending on the lifetime of the involved particles, which can be adjusted by the structure design and the choice of material. In the weak coupling regime the MC enhances the decay of the electronic system via the Purcell-effect, which is exploited in resonant-cavity LEDs (RCLEDs) [2] and conventional short-cavity lasers (VCSEL) [3]. In contrast to this, in the strong coupling regime the interaction strength between excitons and cavity-photons overcomes the losses, yielding stable bosonic quasi-particles (exciton-polaritons) [4,5]. Under certain circumstances, these can form a macroscopic coherent quantum state, so-called dynamical Bose-Einstein Condensates. This enables the investigation of quantum effects in a fundamental way and paves the way for new optoelectronic devices [6].

### Experimental setup

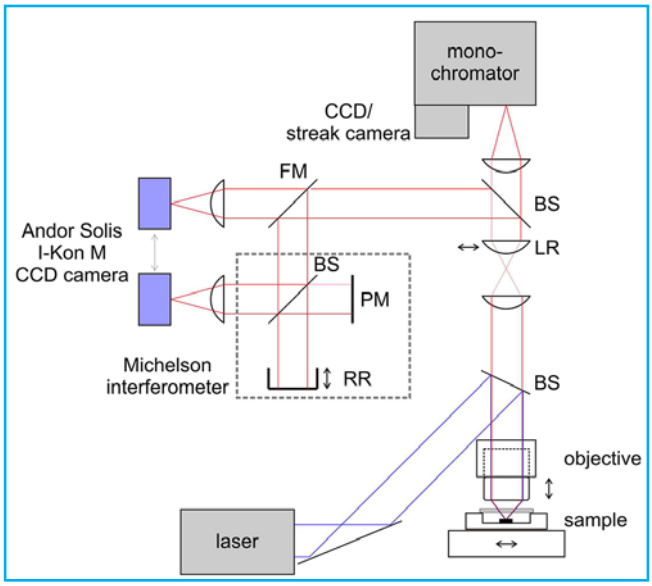


Figure 1: Scheme of the µ-PL imaging setup. BS stands for beamsplitter, FM is a flip mirror, PM means plan mirror and RR denotes a retroreflector. The moveable lens LR enables a fast switching between near-field (with LR) and far-field (without LR) imaging of the PL emission.

In order to assess the optical properties of one- and two-dimensionally confined MC structures we use a photoluminescence (PL) setup with micrometer resolution (µ-PL) as shown in Figure 1. The MC luminescence is excited by a laser emitting in the UV spectral range. This is necessary to excite carriers into the conduction bands of ZnO, which is the cavity material of all our MC structures. The laser beam is focussed by an infinity-corrected UV objective onto the sample surface, with a spot size of about 1 µm$^2$. The emitted PL signal is collected by the same objective within an emission angle range of -30° … + 30°.

# µ-Photoluminescence imaging setup

# for optical characterisation of ZnO-based microcavities

M. Thunert, T. Michalsky, M. Wille, S. Richter, H. Franke, C. Sturm, R.Schmidt-Grund, M. Grundmann
Semiconductor Physics Group, Leipzig University, Leipzig, Germany (August 2014)

## Application Note

A variable lens configuration in the detection path enables a fast switching between near-field I(x,y) and the far-field $I(k_x,k_y)$ imaging of the emission. Here, I is the intensity of the PL emission and x and y are the spatial coordinates. Both imaging methods provide complementary information

(I) The near-field image yields insights into the spatial distribution of the emitted luminescence, which enables a correlation between the microstructure and the optical properties. For instance, the spatial intensity distribution as well as the line broadening of the emission from the cavity mode is correlated with the local defect density, whereas the energy distribution yields information about the cavity thickness [7] or the local electronic potential landscape (local fluctuations). The last is important, e.g. for the investigation of disorder effects [8,9]. In bent wire MCs the local deformation potential due to tensile or compressive strain can be determined from the local energy shift of modes across the wire observable in I(x,y) images [10]. By mapping spatial emission energy profiles of planar MC with mesa structures, the shape of the mesa and their functionality as a trap for polaritons can be investigated [7]. Furthermore, near-field imaging in combination with an interferometry setup provides the basis for spatial correlation measurements, which are important to investigate the phase relation within a Bose-Einstein condensate [11].

(II) Analysis of the far-field emission allows us to investigate the dispersion E(k) [12] of cavity or polariton modes as well as their occupation with cavity-photons respective polaritons by mapping I(E,k) [13]. This enables e.g. the investigation of relaxation and propagation processes of condensed exciton-polaritons [14].

For spectral resolution, the emitted light is analysed by an imaging grid monochromator equipped with a CCD array detector. This allows us to observe energy-resolved intensity line scans I(E,x) or $I(E,k_x)$.
For two-dimensional I(x,y) and $I(k_x,k_y)$ imaging we use an Andor Solis I-Kon M camera in our detection system. By help of a beamsplitter we can record simultaneously highly resolved two-dimensional images of the near- or far-field emission and the spectrally resolved I(E,x) and $I(E,k_x)$ line scans. Thus, all needed information can be gained without changes in the alignment of the detection system.

Moreover, the high frame rate of the Andor Ikon-M camera of up to 5 MHz enables an instant observation of the emission, which is essential for a fast and comfortable alignment of the whole setup. The quadratic sensor with 1024 x 1024 pixel allows an effective illumination of the entire CCD array with a high spatial or angular resolution.

For determination of the first-order spatial coherence function $g^{(1)}(r,-r)$ a interferometry setup in mirror-retroreflector configuration [11] is used. Here, the near-field image of one interferometer arm $I_1(x,y)$ is superimposed by the mirror image $I_2(-x,-y)$ of the other. An incremental movement of one interferometer arm with nm-resolution results in a systematic variation of the phase difference between the two superimposed images in the detection plane. This leads to sinusoidal-intensity oscillations for each pixel of the CCD detector following the equation

Hence, the spatial first order coherence function $g^{(1)}(r,-r)$ can be calculated from the amplitude of the normalized intensity function $A_{norm}(r,-r)$.

### Experimental examples

By means of the µ-PL imaging setup described above we are able to investigate the emission properties of one- and two-dimensionally confined MCs. For demonstration, we have chosen two examples:

At first we show the emission properties of a hexagonal shaped ZnO wire MC with a diameter of about 9 µm. As mentioned above, the two-dimensional real space (cf. Figure 2a) and k-space (cf. Figure 2b) images were recorded via the Andor Ikon-M camera. Additional spectral resolution of the one-dimensional k-space spectral emission (cf. figure 1c) was realized with an imaging monochromator as described above.

For the excitation conditions shown here, almost homogeneous emission can be observed over the entire wire area (cf. Figure 2a) as well as for all detectable emission angles (cf. Figure 2b). In this excitation density regime, the observed luminescence originates from the spontaneous decay of excitons. Applying spectral resolution, multiple energy states are visible showing a parabola-like dispersion. By the determination of the energy spacing, they can be identified as WGMs.
As a second example, we present the operation principle of our interferometer setup. Therefore, we superim-

# µ-Photoluminescence imaging setup for optical characterisation of ZnO-based microcavities

M. Thunert, T. Michalsky, M. Wille, S. Richter, H. Franke, C. Sturm, R.Schmidt-Grund, M. Grundmann
Semiconductor Physics Group, Leipzig University, Leipzig, Germany (August 2014)

## Application Note

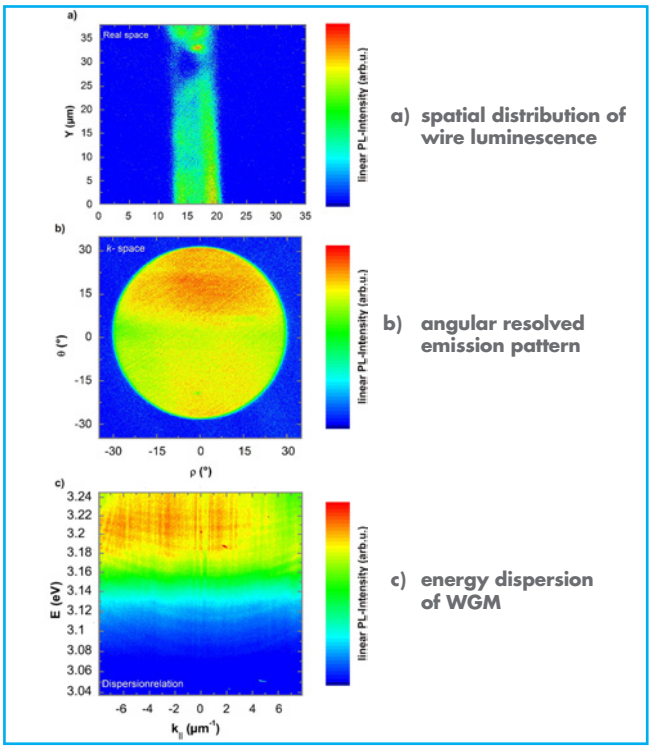


**Figure 2**

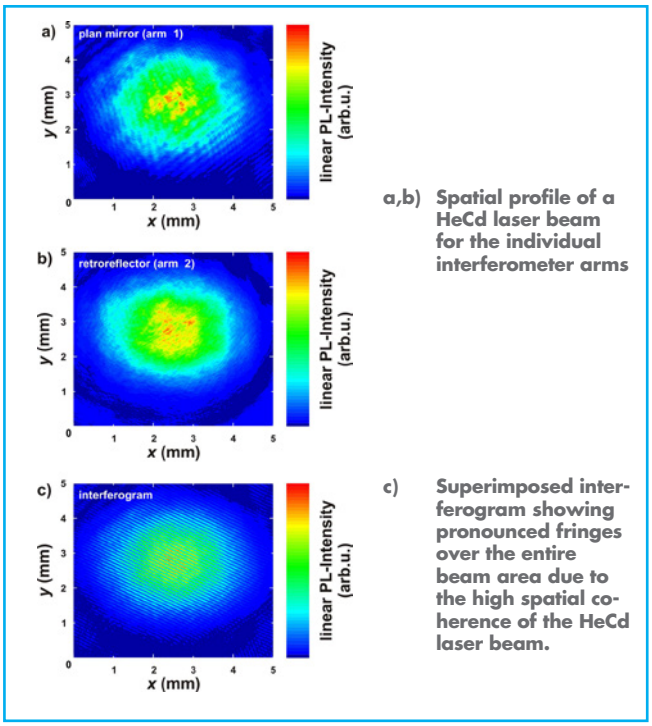


**Figure 3 (All images are recorded by the Andor-Solis I-Kon M camera.)**

posed the original image with the mirror image of the HeCd-laser beam profile as shown in Figure 3. For an incoherent thermal light source such as a conventional light bulb, only interference fringes within the centre of emission would be expected due to autocorrelation of $I_1(r)$ and $I_2(-r)$ for $\Delta r = |r - (-r)| < \lambda_{DB}$ for distances smaller than the thermal de-Broglie wavelength $\lambda_{DB}$.

Note, that the thermal de-Broglie wavelength of carriers created in incoherent light sources is far below one micrometer. For larger distances $\Delta r > \lambda_D B$ the superimposed image of an incoherent light source is the sum of the intensity of both individual arms which corresponds to $g^{(1)}(r,-r) = 0$. In contrast, the interferogram shown in Figure 3c yield interference fringes over the entire beam profile due to the large spatial coherence of the emission of the HeCd laser.

### Summary

We have shown that the simultaneous imaging of the emission profile of MCs onto two different detectors enables a comprehensive investigation of the spatial, angular as well as spectrally resolved PL. On the one hand, an imaging monochromator setup provides spectral resolution e.g. to determine the dispersion of the modes of the MC. On the other hand, the 1024 x 1024 pixel CCD sensor of the Andor Ikon M camera allows us to analyse the two-dimensional emission profile with high spatial or angular resolution. Furthermore, alignment of the setup can be easily done by help of the Andor-Solis Ikon-M camera. The high frame rate of 5 MHz enables an instantaneous observation of the emission, which is essential for a fast and comfortable alignment of the interferometer setup. Furthermore, the quadratic sensor with 1024 x 1024 pixels enables an effective illumination of the entire CCD array. This leads to a high spatial or angular resolution of the two-dimensionally resolved far- and near-field images.

### References

[1] R.D. Richtmyer, J. Appl. Phys 10, 391 (1939).
[2] E. F. Schubert et al., Appl. Phys. Lett. 60, 921 1992).
[3] R. S. Geels et al., Appl. Phys. Lett. 57, 1605 (1990).
[4] S. I. Pekar, Sov. J. Exp. Theor. Phys 6, 785 (1958).
[5] J. J. Hopfield, Phys. Rev. 112, 1555 (1958) .
[6] H. Deng et al., Rev. Mod. Phys. 82, 1489 (2010).

# µ-Photoluminescence imaging setup for optical characterisation of ZnO-based microcavities

M. Thunert, T. Michalsky, M. Wille, S. Richter, H. Franke, C. Sturm, R.Schmidt-Grund, M. Grundmann
Semiconductor Physics Group, Leipzig University, Leipzig, Germany (August 2014)

## Application Note

[7] H. Franke: "PLD-grown ZnO based Microcavities for Bose-Einstein Condensation of Exciton-Polaritons", Ph.D. Thesis, Universität Leipzig (2012) http://www.qucosa.de/recherche/frontdoor/?tx_slubopus4frontend[id]=urn:nbn:de:bsz:15-qucosa-98174
[8] A. Baas et al., Phys. Rev. Lett. 100, 170401 (2008).
[9] D. N. Krizhanovskii et al., Phys. Rev. B 80, 045317 (2009).
[10] C. P. Dietrich et al., Appl. Phys. Lett. 98, 031105 (2011).
[11] J. Kasprzak et al., Nature 443, 409 (2006).
[12] C. Sturm et al., New J. Phys. 11, 073044 (2009).
[13] C. Sturm et al., New J. Phys. 13, 033014 (2011).
[14] H. Franke et al., New. J. Phys. 14, 013037 (2012).

**Contact**

Prof. Marius Grundmann
Universität Leipzig
Institute for Experimental Physics II
Semiconductor Physics Group
Linnéstraße 5
04103 Leipzig, Germany

E-Mail: grundmann@physik.uni-leipzig.de
Phone: +49 341 97-32650
Web: http://www.uni-leipzig.de/~hlp/